Effectiveness of a Test Procedure for Pedestrian Lower Limb Protection in Pedestrians of Various Sizes

Yukou Takahashi, Hiroyuki Asanuma, Iwao Imaizumi

Abstract Standardized test procedures to evaluate safety performance of cars normally represent real-world accidents through specific test conditions. It is important, therefore, to understand how performance improvement under such test conditions influences performance in real-world accidents, which are of course not perfectly represented by such test conditions. The goal of this study is to quantitatively assess how the reduction in pedestrian lower limb injury measures in a standardized subsystem test procedure influences injury measures for pedestrians of different sizes. Three simplified car models, each incorporating two different stiffness characteristics, were used to run impact simulations at 40 km/h against three human finite element (FE) models in different sizes. The direction of change in injury measures was consistent between different pedestrian sizes. The comparison of the change of the peak values of tibia bending moment and knee MCL elongation normalized by the scaled threshold values showed that the change decreases as the size of the pedestrian decreases. It was also found that peak injury measures in different pedestrian sizes can be better estimated when those from a standard anthropometry are scaled under the assumption that contact stiffness between vehicle front-end structures and a pedestrian does not scale, rather than when elastic modulus was assumed not to scale.

Keywords Elderly, human model, lower limb injuries, pedestrian, subsystem test

I. INTRODUCTION

Pedestrian safety is one of the most significant issues in traffic safety worldwide. In 2013, there were 1.25 million road traffic deaths globally. Pedestrians accounted for 22% of fatalities globally. In country terms, pedestrians account for 22.5% of fatalities in Spain, 14.2% in France, 16.7% in Germany, 22.9% in UK, 14.1% in USA, 13.2% in Australia, 26.1% in China, 38.9% in South Korea and 36.2% in Japan of all traffic fatalities [1]. Pedestrian accidents also accounted for 8.0% of all injuries due to traffic accidents in Japan in 2015 [2].

In order to address passive safety performance of cars against pedestrians, the European Enhanced Vehicle-safety Committee (EEVC) has developed subsystem test procedures for the adult and child head, adult upper leg and adult lower leg [3]. Similar to other crash tests, the test procedures employ particular test conditions to represent real-world car–pedestrian accidents. Specifically, the adult and child headform tests are conducted by impacting various locations on the surface of a car within a certain range of wrap-around distance across the width of the car in order to simulate various pedestrian heights. In contrast, the adult upper and lower legform tests only represent a pedestrian of an average adult male size, with impact locations varied only laterally to a car. Due to representation and simplification of car–pedestrian impact scenarios, it is important to understand real-world effectiveness of the improvement in car safety estimated from such representative test procedures.

Some of the past studies have investigated the correlation between pedestrian safety performance of a car evaluated by means of the subsystem tests conducted by the European New Car Assessment Program (Euro NCAP) and the probability of injury in real-world pedestrian accidents. Liers [4] investigated 667 frontal pedestrian accidents from the German In-Depth Accident Study (GIDAS) database and assigned sources of AIS2+ injuries to 60 test zones defined on the car involved in each individual accident, using the Euro NCAP procedure. The reduction of the number of MAIS2+ injured pedestrians was estimated by assuming both the distribution of the color rating over the 60 test zones and the reduction in injury severity (AIS level) as a function of the color

Y. Takahashi is Chief Engineer (e-mail: yukou_takahashi@n.t.rd.honda.co.jp; tel: +81-28-677-3311), H. Asanuma is Engineer and I. Imaizumi is Assistant Chief Engineer, all at Honda R&D Co., Ltd. Automobile R&D Center, Japan.

rating. As the effect of improving Euro NCAP rating on the reduction of injury severity was predefined by the assumption, no technical information has been provided by the study as to how high performance cars evaluated by the test procedure using a specific test condition perform in real-world accidents involving a variety of different impact conditions based on car–pedestrian interaction. Strandroth *et al*. [5] investigated the correlation between Euro NCAP pedestrian rating scores and injury outcome in real-life car–pedestrian crashes. ICD and AIS codes were identified for a total of approximately 500 pedestrians admitted to a hospital from the Swedish Traffic Accident Data Acquisition (STRADA) during 2003–2010. Correlation was investigated between the Euro NCAP score of the car involved in each specific accident and the Risk of Serious Consequences (RSC) defined in the study as a function of the risk of permanent medical impairment from a preceding study. Although actual Euro NCAP test results were applied to the analysis, a focus was given to the statistical significance of the decrease in injury severity due to improvement in Euro NCAP rating. Despite the fact that these studies have statistically clarified the overall real-life effectiveness of performance improvement when the performance is represented by the Euro NCAP score, it has not been quantified as to how the performance improvement of a particular car measured under a representative test condition is effective in impact conditions that are not represented by the representative test condition.

The focus of this study was to assess effectiveness of injury reduction when pedestrian size is varied from that represented by the subsystem test procedure, and to investigate a methodology to provide accurate predictions of injury measures from other sizes of pedestrians using those from a pedestrian with the representative size. Lower limb injuries were investigated because the lower leg subsystem test represents only a pedestrian of an average adult male size. In this study, car-pedestrian impact simulations were conducted using simplified car models to represent different geometric and stiffness characteristics, and human FE models to represent different sizes of a pedestrian, in order to quantitatively compare the change in the peak values of lower limb injury measures between different pedestrian sizes. As geometric similarity does not apply for impacts against pedestrians of different sizes due to unchanged size of a car, the influence of a data scaling method on the prediction of peak injury measures for different sizes of pedestrian is also investigated.

II. METHODS

Impact simulations were conducted using three simplified car models representing different car front-end shapes and three human FE models of different sizes. Two different stiffness characteristics were applied to each of the three car models to provide different levels of peak lower limb injury measures. The change of the peak injury measures were compared between three human models for each of the three car models. Two different data scaling methods were applied to the results from the human model of an average adult male size to predict those from the models of different sizes.

Pedestrian Model

The human FE model in a standing position, representing an average adult male, was developed by the authors in a previous study [6] and was scaled for use in this study. The model includes whole-body skeletal tissues, except the head, hands and feet. Due to the lack of validation, the head model was taken from a model representing a pedestrian dummy. The hands and the feet are modeled as rigid bodies for simplicity. The foot model incorporates the talus and the calcaneus, modeled individually as rigid bodies connected by joints to represent different centers of rotation in dorsiflexion/plantarflexion and inversion/eversion. The model components were individually validated against human response data, including head drop, volunteer head-neck kinematics in frontal and lateral impacts, frontal and oblique thoracic impacts, dynamic lateral compression of isolated pelves, quasi-static and dynamic lateral three-point bending of the thigh, leg, femur, tibia and fibula, quasi-static and dynamic tension of individual knee ligaments, dynamic three-point and four-point bending of the knee and dynamic dorsiflexion/plantarflexion and inversion/eversion of the ankle [6].

The model was scaled to develop three pedestrian models in different sizes. Although the model was developed using CT scan images from a volunteer close to a 50th percentile male, a baseline model was developed representing the exact height and weight of this size, along with the models representing a smaller and a larger size. Due to the importance of protecting elderly pedestrians in Japan, the target height and weight

of the smaller-size pedestrian model were determined to represent the average values of Japanese elderly (65 years old and older, male and female), calculated from a 2012 national health and nutrition survey conducted by the Ministry of Health, Labour and Welfare of Japan [7]. The target height and weight of the baseline and larger-size pedestrian models were determined from the anthropometric study completed by the University of Michigan Transportation Research Institute (UMTRI) [8]. Since the mass of the head is not proportional to the cube of the height scaling factor, the mass of the head for each size was taken from the UMTRI study [8]. The geometry of each of the three models was determined by scaling the model from the previous study [6] using the height scaling factor. Using the individually determined mass of the head, the total mass of these models was modified to match the target weight by tuning the mass density of the flesh. Figure 1 illustrates the three pedestrian models used in this study. Table I summarizes the weight (head and total) and height of the three pedestrian models.

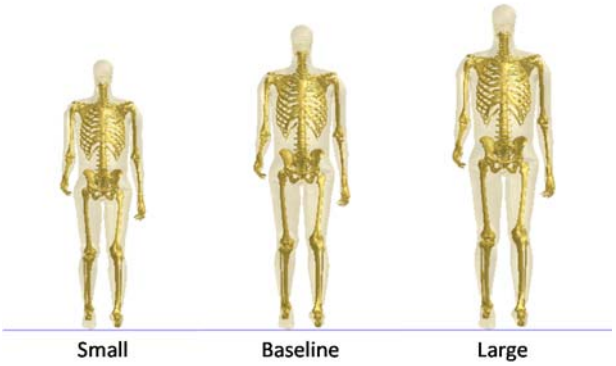

Fig. 1. Human FE models in three sizes.

TABLE I
HEIGHT AND WEIGHT OF HUMAN MODELS

Model	Size Representation	Weight (kg)		Height (cm)
		Head	Total	
Baseline	50th percentile male	4.207	76.7	175.1
Small	Average Japanese elderly (65+ YO)	3.765	55.9	155.2
Large	95th percentile male	4.456	102.6	186.4

Simplified Car Model

The geometry of the three models (S1, S2 and S6) was taken from the 18 simplified car models developed and used in previous studies [9-12]. Figures 2 and 3 show the schematics of the simplified car model and the definition of geometric parameters, respectively. The bumper (BP) and the spoiler (SP) were modeled as rigid bodies. The mass of each BP and SP was set at 16.8 g, determined as the minimum mass to avoid numerical instability. These rigid bodies were connected to a node with a mass of 1500 kg via joint elements, for which force-deflection characteristics in the longitudinal direction of the car were applied. Energy absorption of 90% was applied to unloading for BP and SP, using an exponential unloading curve definition with no residual deflection. The bonnet leading edge (BLE) was modeled by deformable shell elements representing a sheet metal structure made of steel. The mass density, Poisson's ratio and yield stress for BLE were set at 7810 kg/m^3, 0.3 and 3.71 GPa, respectively. Both lateral ends of BLE were rigidly connected to the node representing the mass of a car. As the interaction between these car components and the struck-side limb of a pedestrian significantly affects their interaction with the contralateral limb due to distributed or uniform deformation, each of the components was doubly defined and a contact was defined with one limb each.

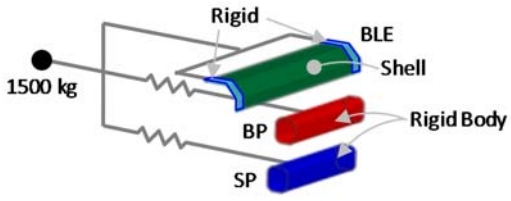

Fig. 2. Schematic of simplified car model [11].

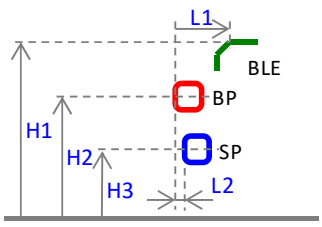

Fig. 3. Definition of geometric parameters [11].

For each of the three models, two sets of stiffness characteristics (Stiffness-A and Stiffness-B) were determined to provide significantly different magnitude of peak lower limb injury measures for the baseline pedestrian model. The stiffness of BLE was controlled by changing the elastic modulus. The stiffness of BP and

SP was changed by applying different loading curves. As a result, a total of six simplified car models were developed. Table II summarizes the geometric parameters and stiffness characteristics of BLE for the six car models. For each of the three shapes (S1, S2 and S6), the models with Stiffness-A and Stiffness-B (shown as the alphabet in the model name) represent deformation characteristics producing lower and higher peak lower limb injury measures, respectively. Since both tibia bending moment and MCL elongation are generated by bending of the leg and the knee, the direction of the change of the stiffness is generally opposite between BP and SP (softer BP located near the knee and stiffer SP located near the distal leg would decrease bending of the knee and the leg). Relative to the geometry represented by S1, all three components are positioned higher from the ground, and BLE and SP are positioned rearward relative to BP. S6 represents a car shape with the same BP and SP heights as those of S1, while the vertical position of BLE is the highest among the three models. The longitudinal distances from BP to BLE and SP are the same as those of S2. Figure 4 presents loading curves for BP and SP specified in S1, S2 and S6. Two sets of loading curves are shown for each component. The curves for Stiffness-A and Stiffness-B are identical for BP specified in S1.

TABLE II
GEOMETRIC AND BLE STIFFNESS PARAMETERS

Model	BLE elastic modulus (GPa)	H1 (mm)	H2 (mm)	H3 (mm)	L1 (mm)	L2 (mm)
S1A	103.0	650	450	250	125	-20
S1B	412.0					
S2A	206.0	700	490	270	200	0
S2B	20.6					
S6A	206.0	750	450	250	200	0
S6B	20.6					

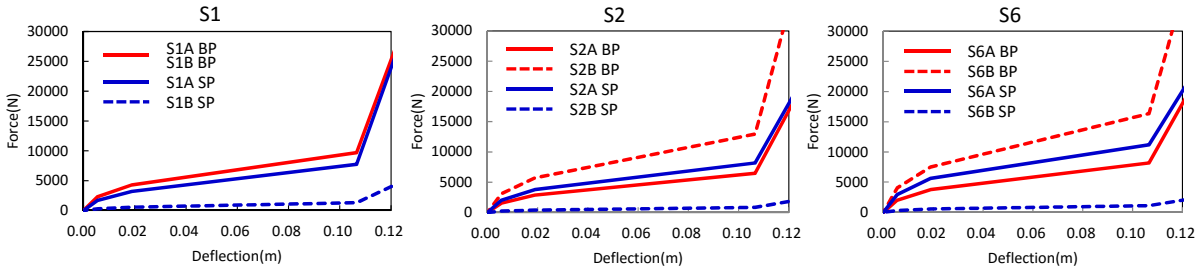

Fig. 4. Loading curves for BP and SP.

Impact Simulation

Three pedestrian models were subjected to impact from six simplified car models laterally from the left at 40 km/h. Untaroiu *et al*. [13] determined the angle of the right and left shoulder, elbow, hip, knee and ankle as a function of the gait parameter, which corresponds to the percentage within one gait cycle, with the initial posture defined as the stance corresponding to the initial contact of the right foot with the ground. This study represented a pedestrian posture with the gait parameter of 50% (stance in mid-gait cycle). Figure 5 shows an example setup of the impact simulation for the baseline pedestrian model and S1 of the simplified car model. In order to present locations of car components relative to a pedestrian body for the three pedestrian sizes, Figure A1 in Appendix illustrates the impact simulation setup in a frontal view of a car model for a total of nine combinations of three simplified car models (S1, S2 and S6) and three pedestrian sizes (Small, Baseline and Large). Table III presents the joint angles (positive in flexion/dorsiflexion) in mid-gait cycle from Untaroiu *et al*. [13] used to define the posture of the pedestrian models.

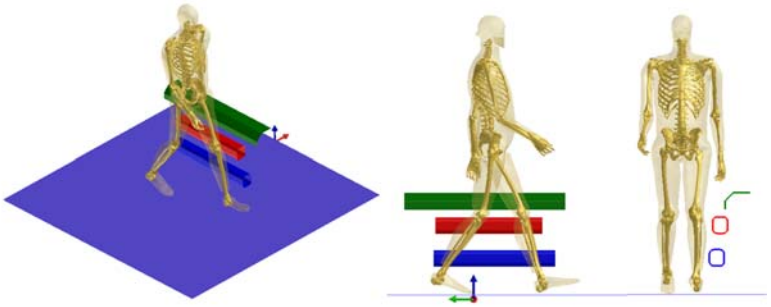

Fig. 5. Impact simulation setup.

TABLE III
JOINT ANGLES FOR STANCE IN MID-GAIT CYCLE

Joint	Angle (deg)	
	Right	Left
Shoulder	19.7	-4.3
Elbow	45.9	18.9
Hip	-13.0	22.7
Knee	21.2	6.0
Ankle	-19.2	2.5

This study used tibia bending moment and knee medial collateral ligament (MCL) elongation on a struck-side limb as lower limb injury measures because these are the measures evaluated by the lower leg-to-bumper subsystem tests using the Flexible Pedestrian Legform Impactor (FlexPLI) as defined by 01 series of amendments to the UN Regulation No. 127 [14]. Tibia bending moment was measured at the cross-section corresponding to the most proximal of the four measurement locations of the FlexPLI because the maximum bending moment is normally reached by this cross-section. For each of the simplified car model geometry (S1, S2 and S6), peak injury measures were compared between two sets of stiffness characteristics to investigate consistency of the change of the peak values between different pedestrian sizes. In order to quantitatively compare the change of the peak injury measures, the peak values were normalized by the threshold values. The threshold values for the baseline model were calculated using the injury probability functions for tibia fracture and MCL failure from Takahashi *et al*. [15] in order to correspond to the threshold values for the FlexPLI specified in 01 series of amendments to the UN Regulation No. 127 [14]. The threshold values for the small and large models were scaled from those of the baseline model using an equal stress/equal velocity scaling method devised by Eppinger *et al*. [16]. Table IV summarizes the threshold values used in this study.

TABLE IV
THRESHOLD VALUES OF LOWER LIMB INJURY MEASURES USED FOR NORMALIZATION

Injury Measures	Pedestrian Model		
	Baseline	Small	Large
Tibia Bending Moment (Nm)	328	228	396
MCL Elongation (mm)	17.3	15.3	18.4

Data Scaling Method

In real-world car–pedestrian accidents, the same car model may collide with pedestrians of different sizes. This justifies the headform test procedure where test points on a car are positioned at various wrap around distances to cover various sizes of pedestrian. As the legform used in the lower leg-to-bumper test represents the lower limb of an average-sized adult male, the effectiveness of reducing peak injury measures would depend on the size of a pedestrian because the size of a car is constant, thus geometric similarity does not perfectly apply. In addition to the clarification of the effectiveness of injury reduction in different pedestrian sizes, this study investigated a methodology to predict peak injury measures in different pedestrian sizes from the results of an average adult male.

When geometric similarity fully applies, the equal stress/equal velocity scaling method by Eppinger *et al*. [16] should work well because the pedestrian models in different sizes used in this study applied exactly the same material property of each of the tissues as well as almost the same mass density, although the mass density of the flesh was slightly modified to exactly match the target weight for each size. This method was used as the first option of the scaling method (Scaling Method-1). In this option, the following fundamental scaling factors were used:

$$\lambda_L = \frac{L}{L_0},\ \lambda_\rho = \frac{\rho}{\rho_0} = 1,\ \lambda_E = \frac{E}{E_0} = 1 \tag{1}$$

where λ is scaling factor, with the suffixes L, ρ and E representing length, mass density and elastic modulus, respectively, L and L_0 are characteristic length, ρ and ρ_0 are mass density, E and E_0 are elastic modulus, with the suffix 0 representing the values for the baseline model. As the pedestrian models were geometrically scaled using the same scaling factor in all three directions, pedestrian height was used as the characteristic length. In this study, tibia bending moment and MCL elongation are used as lower limb injury measures. Given the assumptions described in Equation (1) above, the resulting scaling factors for tibia bending moment and MCL elongation are given by the following equations:

$$\lambda_{tibia} = \lambda_L^3, \ \ \lambda_{MCL} = \lambda_L \tag{2}$$

where λ_{tibia} is tibia bending moment scaling factor and λ_{MCL} is MCL elongation scaling factor.

As geometric similarity does not fully apply due to non-scalable geometry of an impacting car, an alternative method was also used (Scaling Method-2). In this option, an assumption was made that the stiffness (force-deflection) determining the interaction between a car and a pedestrian is the stiffness of a car front structure. Although this option ignores the difference in the stiffness of the lower limb of a pedestrian in a different size, this assumption may incorporate some of the effect of the non-scalable nature of the car geometry by assuming that the stiffness does not scale. This assumption was validated by combining the stiffness curves specified for BP and SP with those for the contact locations on the lower limb of a pedestrian model. The stiffness curves specified for Stiffness-B were used to represent those of BP and SP. The stiffness curves for the lower limb was obtained for the three models by rigidly affixing the middle one fourth of the tibia/fibula to the space and linearly impacting BP and SP individually at 40 km/h with a mass of 1500 kg. Figure A2 in Appendix shows the estimated combined stiffness curves for the six combinations of three car models and two parts (BP/SP), each of which compares the curves obtained from three pedestrian models in different sizes. Since the contact locations of BP and SP on the pedestrian lower limb are near the knee joint and the distal leg, respectively, where the flesh thickness is relatively small, no significant differences were seen between the three pedestrian models except BP of the simplified car model S6. Using the fundamental scaling factors in Equation (1), the stiffness scaling factor λ_K to be assumed 1 in this option is given by the following equation:

$$\lambda_K = \lambda_L \cdot \lambda_E = 1 \tag{3}$$

In this option, only the mass density scaling factor λ_ρ was assumed to be 1, and the elastic modulus scaling factor was determined from Equation (3). The scaling factors for the tibia bending moment and MCL elongation are then given by the following equation:

$$\lambda_{tibia} = \lambda_L^2, \ \ \lambda_{MCL} = \lambda_L \tag{4}$$

These two scaling methods were applied to the peak values of the tibia bending moment and the MCL elongation obtained from the baseline human model to predict those from the small and large models to clarify how these scaling methods work on injury measures. In addition, the maximum value of the impulse calculated from the total force applied to the pedestrian model was also scaled using these two methods in order to figure out how effective these methods are in terms of scaling total momentum transfer, which is deemed less sensitive to the geometric influence of the car front-end structure and pedestrian size.

III. RESULTS

The change in the peak values of tibia bending moment and MCL elongation due to difference in car stiffness characteristics were compared between the three pedestrian models for each of the three simplified car models. Both raw and normalized values were compared. Then the same peak values, as well as the maximum value of the impulse were estimated for the small and large pedestrian models from those of the baseline model using two different scaling methods, and the scaled results were compared with the impact simulation results.

Comparison of Change in Peak Injury Measures

Figures 6 and 7 compare peak tibia bending moment and MCL elongation between two different sets of stiffness characteristics for each combination of the simplified car models (S1, S2 and S6) and the pedestrian models in different sizes (Small, Baseline and Large), respectively. The same comparisons were made for the peak values of the tibia and MCL injury measures normalized by the thresholds presented in Table IV. Figures 8 and 9 show the comparison of normalized tibia bending moment and normalized MCL elongation, respectively. For the tibia bending moment, the reduction of the peak values tended to be smaller as the pedestrian size became smaller, even when the peak values were normalized by the scaled threshold values. In contrast, the change of the peak MCL elongation tended to be larger as the pedestrian size became smaller, as can be clearly seen in S2 and S6.

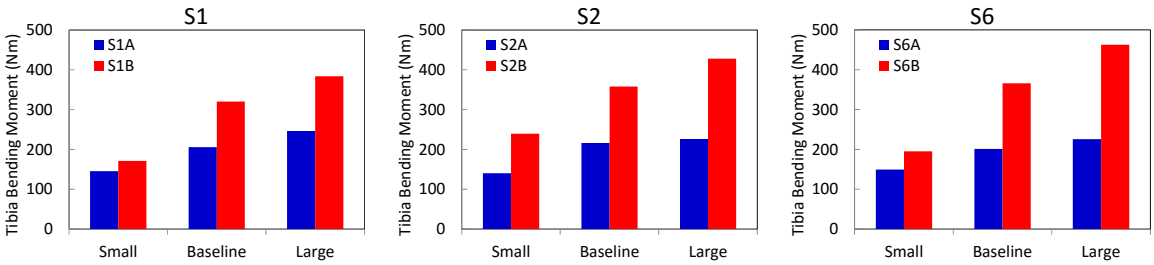

Fig. 6. Comparison of peak tibia bending moment between two sets of car stiffness characteristics.

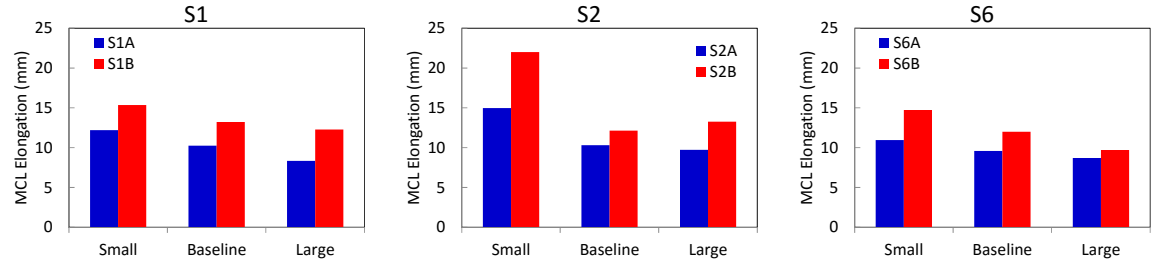

Fig. 7. Comparison of peak MCL elongation between two sets of car stiffness characteristics.

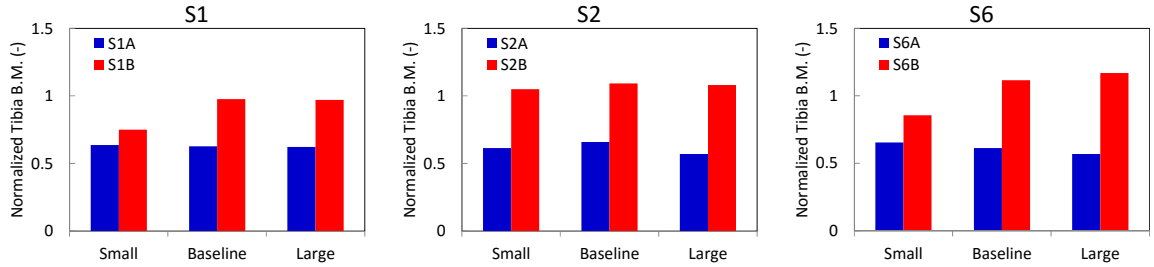

Fig. 8. Comparison of normalized peak tibia bending moment between two sets of car stiffness characteristics.

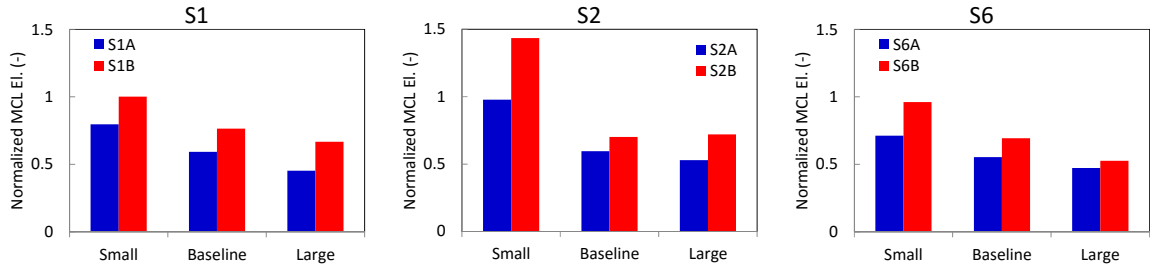

Fig. 9. Comparison of normalized peak MCL elongation between two sets of car stiffness characteristics.

Comparison of Scaled Data with Impact Simulation Results

Figures 10–15 show comparison of raw and scaled peak tibia bending moment, peak MCL elongation and maximum impulse, respectively, for the six combinations of the three simplified car models and the two sets of stiffness characteristics. The results from the two scaling methods (Scaling Method-1, using equal stress/equal velocity method; and Scaling Method-2, assuming force-deflection does not scale) were compared. As for the tibia bending moment, both scaling methods generally work, with Scaling Method-1 providing more accurate prediction in most cases. In contrast, neither of the scaling methods works at all for the MCL elongation, due to the negative trend between peak MCL elongation and height of a pedestrian, as shown in Figs 7 and 9. With regard to the impulse, Scaling Method-2 provided better predictions than Scaling Method-1 in the majority of cases, contrary to tibia bending moment comparisons. These trends are fairly consistent between the three simplified car models with different front-end geometry.

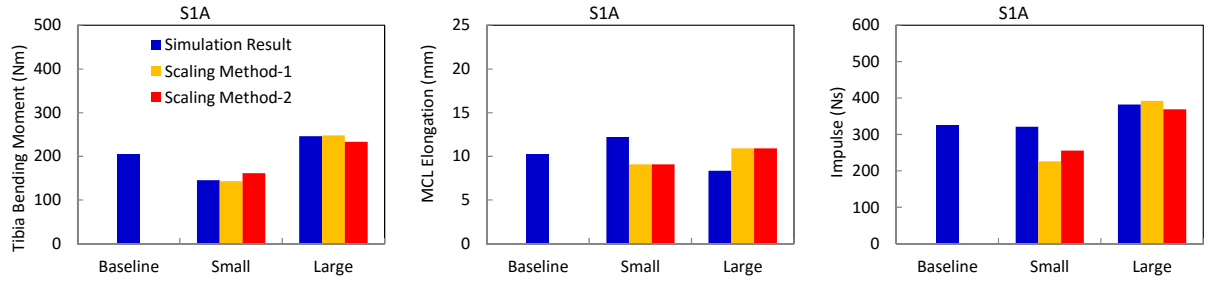

Fig. 10. Comparison of raw and scaled peak tibia bending moment, peak MCL elongation and maximum impulse for simplified car model S1A.

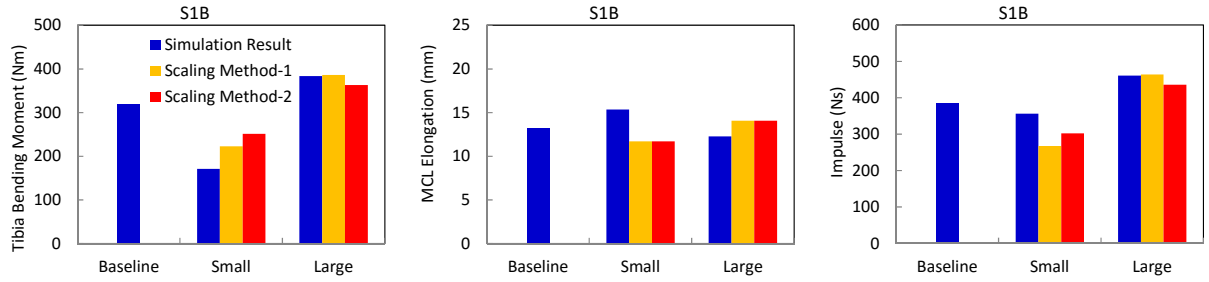

Fig. 11. Comparison of raw and scaled peak tibia bending moment, peak MCL elongation and maximum impulse for simplified car model S1B.

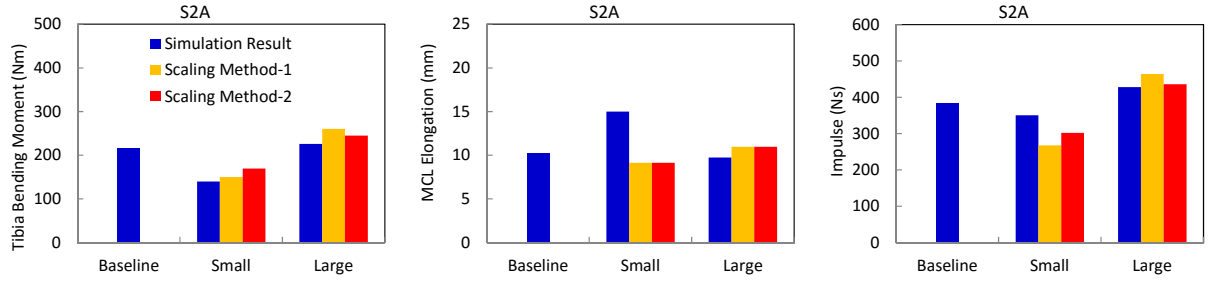

Fig. 12. Comparison of raw and scaled peak tibia bending moment, peak MCL elongation and maximum impulse for simplified car model S2A.

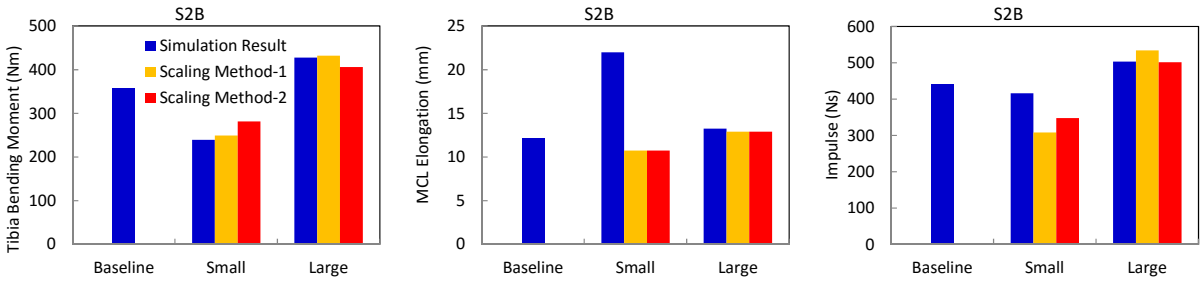

Fig. 13. Comparison of raw and scaled peak tibia bending moment, peak MCL elongation and maximum impulse for simplified car model S2B.

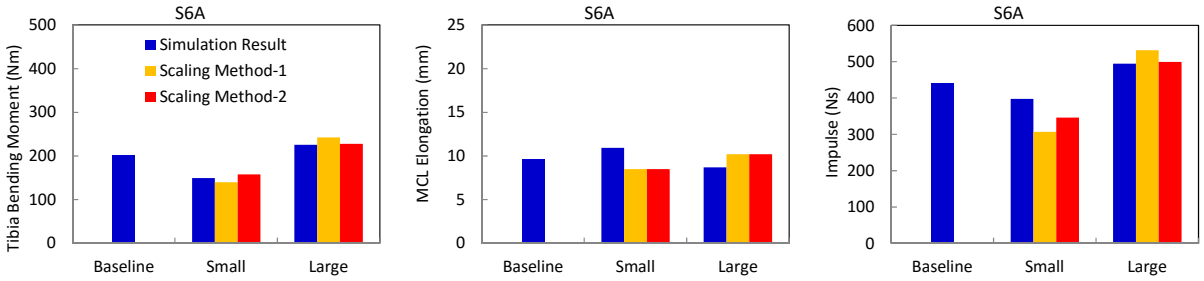

Fig. 14. Comparison of raw and scaled peak tibia bending moment, peak MCL elongation and maximum impulse for simplified car model S6A.

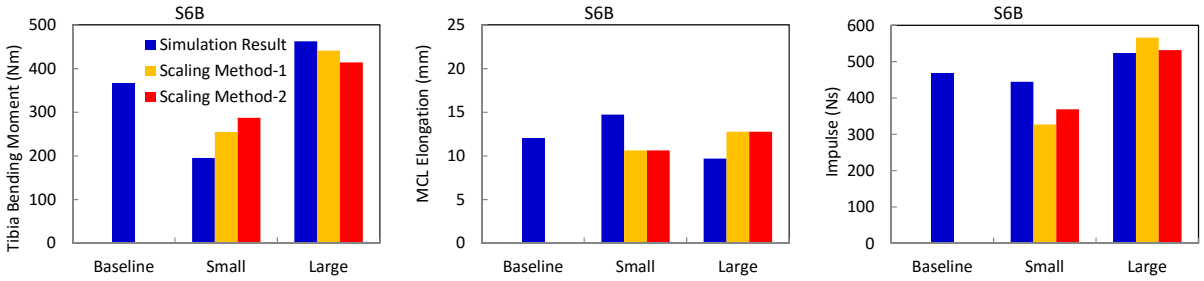

Fig. 15. Comparison of raw and scaled peak tibia bending moment, peak MCL elongation and maximum impulse for simplified car model S6B.

IV. DISCUSSION

In this study, two different sets of stiffness characteristics (Stiffness-A and Stiffness-B) were used for each of three simplified car models (S1, S2 and S6). The results of the impact simulations presented in Figs 6 and 7 show that Stiffness-A provides lower peak values for all three car models and for both lower limb injury measures. This suggests that the change of the car front-end stiffness reducing the peak values of the tibia bending moment and the MCL elongation would be robust enough to reduce them for different sizes of pedestrian not represented by the representative test conditions used by the test procedure.

Normalized reduction of the peak tibia bending moment decreased as the pedestrian size became smaller, as depicted in Fig. 8. This implies that an increased amount of the reduction needs to be achieved in the subsystem test procedure in order for that of a smaller pedestrian to achieve the same percentage of reduction. Normalized reduction of peak MCL elongation did not show any consistent trend when the size of the pedestrian was varied (Fig. 9).

With regards to prediction of peak injury measures for different sizes of pedestrian, from the results of the baseline size shown in Figs 10–15, both scaling methods used in this study worked for the tibia bending moment to some degree, irrespective of geometric and stiffness characteristics of a car, with Scaling Method-1 (equal stress/equal velocity) providing slightly more accurate predictions. In contrast, the scaling methods adjusted the peak value of the MCL elongation in the opposite direction relative to that of the baseline model, due to the

negative correlation between the peak MCL elongation and the height of the pedestrian, as shown in Fig. 7. This suggests that geometric effect would be a predominant factor of determining the peak MCL elongation, and the scaling methods based on geometric similarity would not work well. As shown in Figs 6 and 7, the MCL elongation is generally much less sensitive to the size of a pedestrian compared to the tibia bending moment, with the exception of the car model S2. The height of BP (490 mm) is higher than the other two models (450 mm), as summarized in Table II. The heights of the knee joint for the small, baseline and large pedestrian models were 470 mm, 520 mm and 570 mm, respectively. Therefore, BP contacts above the knee joint only when the car model S2 collides with the small pedestrian model. This could explain the exceptionally high peak MCL elongation in this condition because the knee would experience more valgus bending when one of the two applications of the force to the leg moves above the knee, and the leg tends to rotate underneath the BP. Since this is also a geometric issue, it would be necessary to investigate a scaling procedure based on the geometry of a car front-end and a pedestrian lower limb to predict peak MCL elongation in different sizes of pedestrian.

Contrary to the better prediction of peak tibia bending moment with Scaling Method-1, Scaling Method-2 provided better predictions for maximum impulse in all conditions, except the car model S1 against the large pedestrian model. This implies that the scaling method assuming a constant force-deflection involved in a collision would more accurately scale momentum transfer from a car to the pedestrian lower limb. It is also suggested that the slightly better predictions of the peak tibia bending moment from Scaling Method-1 would mean that geometric effect also plays a role in determining the peak tibia bending moment.

This study only investigated the effectiveness of reduction in the peak lower limb injury measures in different pedestrian sizes for three car front-end shapes at the impact speed of 40 km/h. It would be needed to investigate the influence of the orientation, posture and material property of a pedestrian body, more variations in car shapes and different impact speeds to draw more comprehensive conclusions. The whole-body kinematics and kinetics in car impacts was validated only for the original model, which requires further validation of scaled models in a future study when more human response data are available.

In this study, only the influence of pedestrian sizes on the effectiveness of injury mitigation was investigated. Although the small size pedestrian used in this study represented that of an average Japanese elderly, it is important to note that only the height and weight of such a population were represented, without incorporating difference in material properties due to aging. Although an injury probability function developed as a function of age would allow some estimation of the probability of injuries in the elderly, the impact responses would differ with different material parameters, thus a more comprehensive study is needed to further clarify injuries to the elderly. It should also be noted that the current study employed simplified car models, not actual car models. Although similar results are expected to be seen with actual car models due to representation of major front-end structures that apply loads to a pedestrian during an impact, the results obtained from this study need to be validated against actual cars in a future study.

V. CONCLUSIONS

This study conducted impact simulations of three simplified car models, each with two stiffness characteristics, against three human FE models of different sizes at 40 km/h. The changes in the peak lower limb injury measures were compared. In addition, two different data scaling methods were applied to the results from the human model of an average-size adult male to predict those from the models of different sizes. The following conclusions were reached as a result of this study.

- The change of the car front-end stiffness reducing the peak values of the tibia bending moment and the MCL elongation for an average adult male also reduced them for different sizes of pedestrian for all three car models.
- Normalized reduction of the peak tibia bending moment decreased as the pedestrian size became smaller.
- Normalized reduction of peak MCL elongation did not show any consistent trend when the size of a pedestrian was varied.
- Both scaling methods used in this study reasonably predicted the tibia bending moment in different pedestrian sizes, irrespective of geometric and stiffness characteristics of a car.
- The scaling methods adjusted the peak MCL elongation in the opposite direction relative to that of the baseline model, due to the negative correlation between the peak MCL elongation and the height of a pedestrian.

- The maximum impulse was better predicted with a scaling method assuming that the stiffness (force-deflection) does not scale.

VI. REFERENCES

[1] World Health Organization. (2015) Global Status Report on Road Safety 2015.

[2] Institute for Traffic Accident Research and Data Analysis. (2015) Traffic Accident Statistics 2015 (in Japanese).

[3] European Enhanced Vehicle-safety Committee. (1998) EEVC Working Group 17 Report - Improved test methods to evaluate pedestrian protection afforded by passenger cars.

[4] Liers, H. Benefit Estimation of the Euro NCAP pedestrian rating concerning real world pedestrian safety. Proceedings of 21st ESV Conference, 2009, Stuttgart (Germany), Paper Number 09-0387.

[5] Strandroth, J., Rizzi, M., Sternlund, S., Lie, A., Tingvall, C. (2011) The Correlation Between Pedestrian Injury Severity in Real-Life Crashes and Euro NCAP Pedestrian Test Results. *Traffic Injury prevention*, **12**(6): pp.604–13.

[6] Takahashi, Y., Asanuma, H., Yanaoka, T. Development of a Full-Body Human FE Model for Pedestrian Crash Reconstructions. *Proceedings of IRCOBI Conference*, 2015, Lyon (France).

[7] Ministry of Health, Labour and Welfare. (2013) National Health and Nutrition Survey 2012 (in Japanese).

[8] Robbins, D.H. (1983) Anthropometric Specifications for Mid-sized Male Dummy, Volume 2. The University of Michigan Transportation Research Institute, Report Number UMTRI-83-53-2.

[9] Konosu, A., Issiki, T., Tanahashi, M., Suzuki, H. Development of a Flexible Pedestrian Legform Impactor Type GT (Flex-GT). *Proceedings of 20th ESV Conference*, 2007, Lyon, France, Paper Number 07-0178.

[10] Konosu, A., Issiki, T., Takahashi, Y. Evaluation of the Validity of the Tibia Fracture Assessment using the Upper Tibia Acceleration Employed in the TRL Legform Impactor. *Proceedings of IRCOBI Conference*, 2009, York (UK).

[11] Takahashi, Y., Ikeda, M., Imaizumi, I., Kikuchi, Y., Takeishi, S. Validation of Pedestrian Lower Limb Injury Assessment using Subsystem Impactors. *Proceedings of IRCOBI Conference*, 2012, Dublin (Ireland).

[12] Takahashi, Y., Imaizumi, I., Asanuma, H., Ikeda, M. Responses of the Flexible Legform Impactor in Car Impacts. *Proceedings of IRCOBI Conference*, 2013, Gothenburg (Sweden).

[13] Untaroiu, C., Meissner, M. *et al*. (2009) Crash reconstruction of pedestrian accidents using optimization techniques. *International Journal of Impact Engineering*, **36**(2): pp.210–19.

[14] United Nations. Addendum 126: Regulation No. 127 – 01 series of amendments to the Regulation, 2015, Document Number E/ECE/324/Rev.2/Add.126/Rev.1−E/ECE/TRANS/505/Rev.2/Add.126/Rev.1.

[15] Takahashi, Y., Matsuoka, F., Okuyama, H., Imaizumi, I. (2012) Development of Injury Probability Functions for the Flexible Pedestrian Legform Impactor. *SAE International Journal of Passenger Cars - Mechanical Systems*, **5**(1): pp.242–52.

[16] Eppinger, R. Prediction of Thoracic Injury Using Measurable Experimental Parameters. *Proceedings of the International Conference on Experimental Safety Vehicles*, 1976, London (UK).

VII. APPENDIX

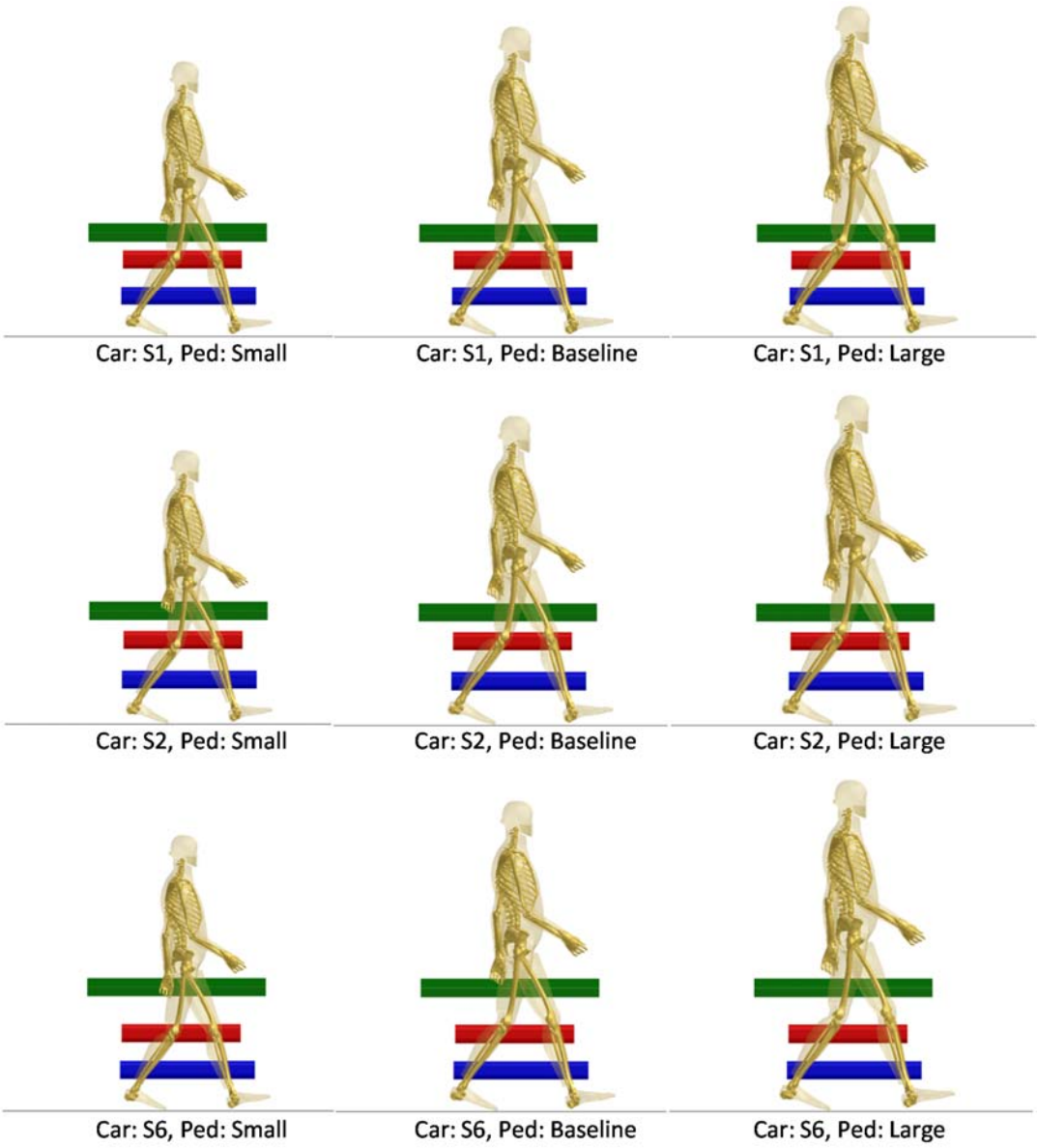

Fig. A1. Impact simulation setup for all combinations of three simplified car models and three pedestrian models.

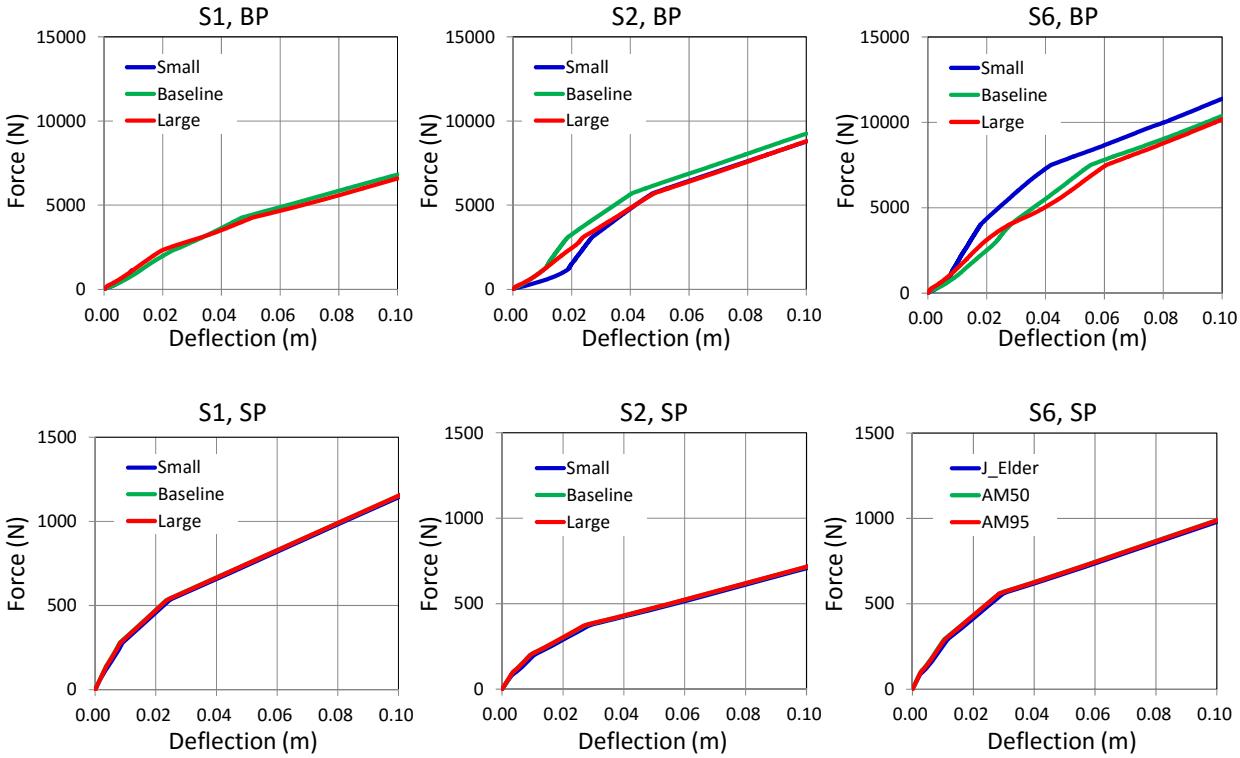

Fig. A2. Comparison of combined stiffness curves between pedestrian models in different sizes.